Contemporary Engineering Sciences, Vol. 9, 2016, no. 14, 689 - 704
HIKARI Ltd, www.m-hikari.com
http://dx.doi.org/10.12988/ces.2016.6432

Elastic Characteristics of a Non-Symmetric Laminated Composite Roller Guided Panel through Mathematical Approach

Jaegwi Go

Department of Mathematics, Changwon National University
20 Changwondaehak-ro Uichang-gu, Changwon, Gyeongnam 641-773, Korea

Je-Hyun Lee

School of Nano and Advanced Materials Engineering
Changwon National University
20 Changwondaehak-ro Uichang-gu, Changwon, Gyeongnam 641-773, Korea

Seokmin Joo

Electrical Engineering, Gimhae College
198, Saman-ro 112 gil, Gimhae-si, Gyeongnam 50811, Korea
Corresponding author

Abstract

Roller guided panel composed of non-symmetric laminated material is taken into account to investigate the elastic characteristics. Two displacement parameters are utilize to formulate derive the plane stress elasticity problem and a pair of partial differential equations are obtained. Due to the complexity of the governing equations a finite element technique is applied to a panel of glass/epoxy laminated composite to search numerical approximation. The profiles of stress and displacement distribution are displayed for various angle sequences and different section of panel and the versatile behaviors appears depending on the location and laminated angle sequence. It is recognized that the mathematical approach is reasonable and the results may be helpful to design an ideally laminated elastic field.

Keywords: Elastic characteristics, Finite element method, Laminated composite materials, Roller guided panel

1 Introduction

Due to the superior strength and stiffness to weight ratios, and high fatigue resistance, composite materials (CM) have been widely applied to engineering applications such as aerospace, marine, wind turbines, and automotive. Various types of structural elements, in many applications, are employed for suitable use, and the structural elements are under the action of both loads and constraint at the same time during the service. Moreover, the appropriate material constitutive models suffer from large deflections and stresses in the presence of inherent scatter in the material properties under random loadings. The credible analysis to failure mechanisms, thus, is a crucial part for reliable performance in applications, and is required to predict their mechanical behavior such as maximum load and the elastic characteristics of laminated CMs.

Composite cylindrical shells, applicable to underground and underwater pipelines boiler tube, and submarine structures, were investigated to analyze the failure mechanisms by [1, 2]. Cylindrical shell models usually experience external hydrostatic pressure. Anastasiadis and Simitses [3] used higher order deformation theory to study the buckling of long laminated cylindrical shells subjecting external radial pressure. A non-linear theory for stretching and bending of anisotropic beams having constant initial curvature in their plane of symmetry was developed for calculating stability limits of thin anisotropic rings/long cylinders [4], and the study to the buckling stability of composite, thin-walled rings/long cylinders under external pressure was extended by Karam [5] introducing radial material grading concept.

Laminated composite plates are commonly used components in aerospace vehicles, automobiles, ships, and trains in designing wings, skins, control surfaces and access panels. Wang and Kam [6] adopted a minimization method based on static test results to study material characterization of laminated composite plates. A first order perturbation technique used by Salim et al. [7] to obtain the second order statistics for static deflection, natural frequency and buckling load of rectangular plates, and Gorman [8] presented free vibration analysis of thin rectangular plates with variable edge supports using the method of superimposition. Monte Carlo Simulation was employed by Raj et al. [9] to analyze rectangular plates with and without cutouts using higher order shear deformation theory, and stochastic finite element method was been adopted by Nakagiri et al. [10] to investigate simply supported graphite/epoxy plates taking fiber orientation, layer thickness and layer numbers as random variables, yielding that the overall stiffness of fiber reinforced composite laminated plates is largely dependent on the fiber orientation.

Meanwhile, the study of elastic characteristics to non-symmetric laminated composites, due to the complexity, has been limited on simple cylindrical and rectangular composite models. Singh et al. [11], and Kumar and Yadav [12] employed Hamilton principle to analyze the elastic behavior of anti-symmetric

rectangular cross-ply plates. Kirchhoff–Love plate theory used by Kumar with Von-Karman nonlinear strain displacement relations to model the system behavior and perturbation approach was applied to develop the system equations to obtain the response statistics of flat plates. In the present study, the analysis of elastic characteristics is extended to a non-symmetric cross-ply laminated composite field guided by roller panel. The elastic field is under the action of mixed boundary loadings. Based on the displacement approach to the laminated composite field problem, a pair of second order partial differential equation is derived. Since the governing equations are too involved to solve analytically, a finite element method is applied to obtain approximated solutions. The expressions of stresses in terms of displacement components are employed to describe the stress behaviors. The results may be applicable to sliding door and window, sliding fences, and sliding sun roofs.

2 Mathematical Modelling

2.1. Mathematical formulation

A rectangular roller guided panel is taken into account for the elastic characteristics of composite materials in two dimensional Cartesian frame (See Fig. 1). The panel is made of non-symmetric cross-ply laminated composite materials, and is under the actions of constraint along the left lateral side and roller guided along the two longitudinal sides of the panel. a and b stand for the width and length of the panel, respectively. The panel is under the action for the followings; (i) A linearly varying tensile load $\sigma_x = P(1-2y/a)$ is applied on the right side, no lateral stress is appeared on roller guided sides, and no displacement is developed on edges perpendicular to roller guided sides, (ii) the bending-extension coupling stiffness matrix vanishes, and (iii) the values of shear-extension coupling terms of the extensional stiffness matrix are zero. P represents the maximum value of the load.

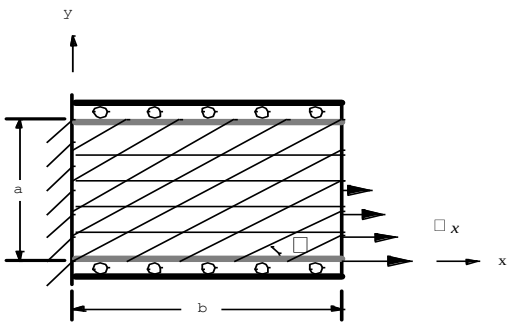

Figure 1. . Schematic view a non-symmetric laminated roller guided panel

Based on the concept of the displacement potential approach for the composite laminated theory, the average stress-strain relations under the plane stress, in global coordinates system, can be written by

$$\begin{bmatrix}\sigma_x\\ \sigma_y\\ \tau_{xy}\end{bmatrix}=\frac{1}{h}\begin{bmatrix}A_{11} & A_{12} & A_{16}\\ A_{12} & A_{22} & A_{26}\\ A_{16} & A_{26} & A_{66}\end{bmatrix}\begin{bmatrix}\varepsilon_x\\ \varepsilon_y\\ \gamma_{xy}\end{bmatrix} \tag{1}$$

σ_x and σ_y are normal stress components in the x- and y- directions, respectively, τ_{xy} the shear stress component, ε_x and ε_y normal strain components the x- and y- directions, respectively, γ_{xy} the shear strain component, and h is the total thickness of the laminate. The elements of stiffness matrix $[A]$ are given by

$$A_{11}=\sum_{k=1}^{n}[Q_{11}\cos^4\theta+Q_{22}\sin^4\theta+2(Q_{12}+2Q_{66})\cos^2\theta\sin^2\theta]_k(h_k-h_{k-1})$$

$$A_{12}=\sum_{k=1}^{n}[(Q_{11}+Q_{22}-4Q_{66})\cos^2\theta\sin^2\theta+Q_{12}(\cos^4\theta+\sin^4\theta)]_k(h_k-h_{k-1})$$

$$A_{22}=\sum_{k=1}^{n}[Q_{11}\sin^4\theta+Q_{22}\cos^4\theta+2(Q_{12}+2Q_{66})\cos^2\theta\sin^2\theta]_k(h_k-h_{k-1})$$

$$A_{16}=\sum_{k=1}^{n}[(Q_{11}-Q_{12}-2Q_{66})\cos^3\theta\sin\theta+(Q_{12}-Q_{22}+2Q_{66})\cos\theta\sin^3\theta]_k(h_k-h_{k-1})$$

$$A_{26}=\sum_{k=1}^{n}[(Q_{11}-Q_{12}-2Q_{66})\cos\theta\sin^3\theta+(Q_{12}-Q_{22}+2Q_{66})\cos^3\theta\sin\theta]_k(h_k-h_{k-1})$$

$$A_{66}=\sum_{k=1}^{n}[(Q_{11}+Q_{22}-2Q_{12}-2Q_{66})\cos^2\theta\sin^2\theta+Q_{66}(\cos^4\theta+\sin^4\theta)]_k(h_k-h_{k-1})\ .$$

Here, (h_k-h_{k-1}) is the thickness of the k-th ply of the laminate, θ is the angle between the x-axis and the fiber direction of a laminate in the laminate, E_1 and E_2 are the Young's modulus in the longitudinal and transverse directions, respectively, ν_1 and ν_2 are the major and minor Poison's ratio, respectively, and G_{12} is the in-plain shear modulus of a laminate in the laminate, and

$$Q_{11}=\frac{E_1}{1-\nu_{21}\nu_{12}},\ Q_{12}=\frac{\nu_{12}E_1}{1-\nu_{21}\nu_{12}},\ Q_{22}=\frac{E_2}{1-\nu_{21}\nu_{12}},\ Q_{11}=G_{12}.$$

The basic stress can be expressed in terms of displacements as

$$\sigma_x=\frac{1}{h}[A_{11}\frac{\partial u_x}{\partial x}+A_{12}\frac{\partial u_y}{\partial y}+A_{16}(\frac{\partial u_x}{\partial y}+\frac{\partial u_y}{\partial x})]$$

$$\sigma_y=\frac{1}{h}[A_{12}\frac{\partial u_x}{\partial x}+A_{22}\frac{\partial u_y}{\partial y}+A_{26}(\frac{\partial u_x}{\partial y}+\frac{\partial u_y}{\partial x})]$$

$$\tau_{xy}=\frac{1}{h}[A_{16}\frac{\partial u_x}{\partial x}+A_{26}\frac{\partial u_y}{\partial y}+A_{66}(\frac{\partial u_x}{\partial y}+\frac{\partial u_y}{\partial x})], \tag{2}$$

where u_x and u_y are the displacement components in the x- and y-directions, respectively. The equation of equilibrium for the plane elasticity problems are given by

$$\frac{\partial \sigma_x}{\partial x} + \frac{\partial \tau_{xy}}{\partial y} = 0$$
$$\frac{\partial \sigma_y}{\partial y} + \frac{\partial \tau_{xy}}{\partial x} = 0\,, \tag{3}$$

where Ω is the blade rotational speed. The combination of Eqs (2) and (3) provides

$$-\frac{\partial}{\partial x}[A_{11}\frac{\partial u_x}{\partial x} + A_{12}\frac{\partial u_y}{\partial y} + A_{16}(\frac{\partial u_x}{\partial y} + \frac{\partial u_y}{\partial x})] - \frac{\partial}{\partial y}[A_{16}\frac{\partial u_x}{\partial x} + A_{26}\frac{\partial u_y}{\partial y} + A_{66}(\frac{\partial u_x}{\partial y} + \frac{\partial u_y}{\partial x})] = 0 \tag{4a}$$

$$-\frac{\partial}{\partial x}[A_{16}\frac{\partial u_x}{\partial x} + A_{26}\frac{\partial u_y}{\partial y} + A_{66}(\frac{\partial u_x}{\partial y} + \frac{\partial u_y}{\partial x})] - \frac{\partial}{\partial y}[A_{12}\frac{\partial u_x}{\partial x} + A_{22}\frac{\partial u_y}{\partial y} + A_{26}(\frac{\partial u_x}{\partial y} + \frac{\partial u_y}{\partial x})] = 0\,. \tag{4b}$$

Due to the above assumptions the boundary conditions for the present roller guided panel shown in Fig. 1 are

$$u_x(0,y) = u_y(0,y) = 0 \quad (0 \le y \le a), \qquad u_y(x,0) = u_y(x,a) = 0 \quad (0 \le x \le b)$$
$$\sigma_{xy}(x,0) = \sigma_{xy}(x,a) = 0 \quad (0 \le x \le b), \qquad \sigma_{xy}(b,y) = 0 \quad (0 \le y \le a)$$
$$\sigma_x(b,y) = P(1 - \frac{2y}{a}) \quad (0 \le y \le \frac{a}{2}) \tag{5}$$

2.2 Finite element formulation

Since the governing equation (4) is too involved to solve analytically, the partial differential equations convert into a linear system based on a finite element method consisting of rectangular element. Now, the variational approach for the equations (4) is developed based on a finite element method. Multiplication equation (4a) by a trial function w_1 and equation (4b) by w_2, and integration over the domain yields the followings:

$$\int_\Omega [\frac{\partial w_1}{\partial x}(A_{11}\frac{\partial u_x}{\partial x} + A_{12}\frac{\partial u_y}{\partial y} + A_{16}(\frac{\partial u_x}{\partial y} + \frac{\partial u_y}{\partial x})) + \frac{\partial w_1}{\partial y}(A_{16}\frac{\partial u_x}{\partial x} + A_{26}\frac{\partial u_y}{\partial y} + A_{66}(\frac{\partial u_x}{\partial y} + \frac{\partial u_y}{\partial x}))]dA = \oint_\Gamma w_1 t_x ds \tag{6a}$$

$$\int_\Omega [\frac{\partial w_2}{\partial x}(A_{16}\frac{\partial u_x}{\partial x} + A_{26}\frac{\partial u_y}{\partial y} + A_{66}(\frac{\partial u_x}{\partial y} + \frac{\partial u_y}{\partial x})) + \frac{\partial w_2}{\partial y}(A_{12}\frac{\partial u_x}{\partial x} + A_{22}\frac{\partial u_y}{\partial y} + A_{26}(\frac{\partial u_x}{\partial y} + \frac{\partial u_y}{\partial x}))]dA = \int_\Gamma w_2 t_y ds \tag{6b}$$

where

$$t_x = n_x(A_{11}\frac{\partial u_x}{\partial x} + A_{12}\frac{\partial u_y}{\partial y} + A_{16}(\frac{\partial u_x}{\partial y} + \frac{\partial u_y}{\partial x})) + n_y(A_{16}\frac{\partial u_x}{\partial x} + A_{26}\frac{\partial u_y}{\partial y} + A_{66}(\frac{\partial u_x}{\partial y} + \frac{\partial u_y}{\partial x}))$$

$$t_y = n_x(A_{16}\frac{\partial u_x}{\partial x} + A_{26}\frac{\partial u_y}{\partial y} + A_{66}(\frac{\partial u_x}{\partial y} + \frac{\partial u_y}{\partial x})) + n_y(A_{12}\frac{\partial u_x}{\partial x} + A_{22}\frac{\partial u_y}{\partial y} + A_{26}(\frac{\partial u_x}{\partial y} + \frac{\partial u_y}{\partial x}))$$

are the tractions on Γ. The domain Ω is divided into sub-domains (see Fig. 2), Ω^e, $e = 1,2,...,N$, and the variational form over the each element Ω^e is

$$\int_{\Omega^e}[\frac{\partial w_1}{\partial x}(A_{11}\frac{\partial u_x}{\partial x} + A_{12}\frac{\partial u_y}{\partial y} + A_{16}(\frac{\partial u_x}{\partial y} + \frac{\partial u_y}{\partial x})) + \frac{\partial w_1}{\partial y}(A_{16}\frac{\partial u_x}{\partial x} + A_{26}\frac{\partial u_y}{\partial y} + A_{66}(\frac{\partial u_x}{\partial y} + \frac{\partial u_y}{\partial x}))]dA = \oint_{\Gamma^e} w_1 t_x ds \quad (7a)$$

$$\int_{\Omega^e}[\frac{\partial w_2}{\partial x}(A_{16}\frac{\partial u_x}{\partial x} + A_{26}\frac{\partial u_y}{\partial y} + A_{66}(\frac{\partial u_x}{\partial y} + \frac{\partial u_y}{\partial x})) + \frac{\partial w_2}{\partial y}(A_{12}\frac{\partial u_x}{\partial x} + A_{22}\frac{\partial u_y}{\partial y} + A_{26}(\frac{\partial u_x}{\partial y} + \frac{\partial u_y}{\partial x}))]dA = \int_{\Gamma^e} w_2 t_y ds \quad (7b)$$

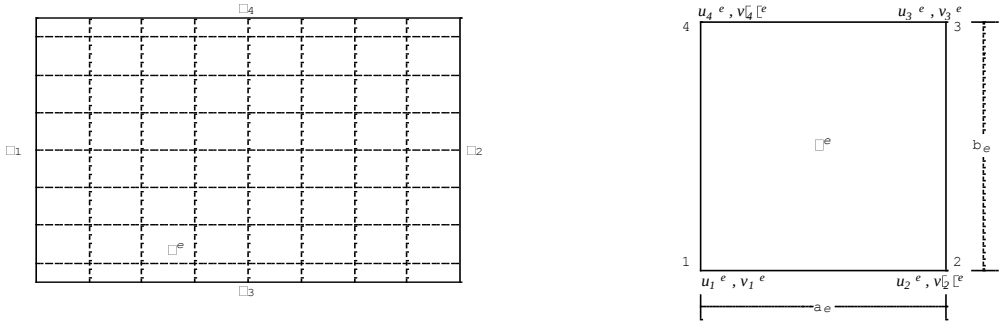

(a) (b)

Figure 2. (a) Discretization of domain, (b) four-node element

Let us define

$$B^{11}(w_1,u_x) = \int_{\Omega^e}[\frac{\partial w_1}{\partial x}A_{11}\frac{\partial u_x}{\partial x} + \frac{\partial w_1}{\partial x}A_{16}\frac{\partial u_x}{\partial y} + \frac{\partial w_1}{\partial y}A_{16}\frac{\partial u_x}{\partial x} + \frac{\partial w_1}{\partial y}A_{66}\frac{\partial u_x}{\partial y}]dA$$

$$B^{12}(w_1,u_y) = \int_{\Omega^e}[\frac{\partial w_1}{\partial x}A_{12}\frac{\partial u_y}{\partial y} + \frac{\partial w_1}{\partial x}A_{16}\frac{\partial u_y}{\partial x} + \frac{\partial w_1}{\partial y}A_{26}\frac{\partial u_y}{\partial y} + \frac{\partial w_1}{\partial y}A_{66}\frac{\partial u_y}{\partial x}]dA$$

$$B^{21}(w_2,u_x) = \int_{\Omega^e}[\frac{\partial w_2}{\partial x}A_{16}\frac{\partial u_x}{\partial x} + \frac{\partial w_2}{\partial x}A_{66}\frac{\partial u_x}{\partial y} + \frac{\partial w_2}{\partial y}A_{12}\frac{\partial u_x}{\partial x} + \frac{\partial w_2}{\partial y}A_{26}\frac{\partial u_x}{\partial y}]dA \quad ,$$

$$B^{22}(w_2,u_y) = \int_{\Omega^e}[\frac{\partial w_2}{\partial x}A_{26}\frac{\partial u_y}{\partial y} + \frac{\partial w_2}{\partial x}A_{66}\frac{\partial u_y}{\partial x} + \frac{\partial w_2}{\partial y}A_{22}\frac{\partial u_y}{\partial y} + \frac{\partial w_2}{\partial y}A_{26}\frac{\partial u_y}{\partial x}]dA$$

$$l^1(w_1) = \oint_{\Gamma_e} w_1 t_x ds, \qquad l^2(w_2) = \oint_{\Gamma_e} w_2 t_y ds,$$

then equations (6) are of the form

$$B^{11}(w_1,u_x)+B^{12}(w_1,u_y)=l^1(w_1),\quad B^{21}(w_2,u_x)+B^{22}(w_2,u_y)=l^2(w_2). \tag{8}$$

Suppose that on an element e

$$u_x \approx \sum_{j=1}^{n} u_j^{(e)}\phi_j^{(e)},\qquad u_y \approx \sum_{j=1}^{n} v_j^{(e)}\phi_j^{(e)}.$$

The $u_j^{(e)}$, $v_j^{(e)}$ are the nodal values of the primary variables. By employing the Ritz method the variational form (7) can be written by

$$\sum_{j=1}^{n} B^{11}(\phi_i^{(e)},\phi_j^{(e)})u_j^{(e)}+\sum_{j=1}^{n} B^{12}(\phi_i^{(e)},\phi_j^{(e)})v_j^{(e)}=l^1(\phi_i^{(e)})$$

$$\sum_{j=1}^{n} B^{21}(\phi_i^{(e)},\phi_j^{(e)})u_j^{(e)}+\sum_{j=1}^{n} B^{22}(\phi_i^{(e)},\phi_j^{(e)})v_j^{(e)}=l^2(\phi_i^{(e)}),$$

or

$$[K^{11(e)}]\{u^{(e)}\}+[K^{12(e)}]\{v^{(e)}\}=\{F^{1(e)}\}$$

$$[K^{21(e)}]\{u^{(e)}\}+[K^{22(e)}]\{v^{(e)}\}=\{F^{1(e)}\}. \tag{9}$$

The matrix elements represent, respectively,

$$K_{ij}^{11(e)}=\int_{\Omega^{(e)}}[A_{11}\frac{\partial\phi_i^{(e)}}{\partial x}\frac{\partial\phi_j^{(e)}}{\partial x}+A_{16}\frac{\partial\phi_i^{(e)}}{\partial x}\frac{\partial\phi_j^{(e)}}{\partial y}+A_{16}\frac{\partial\phi_i^{(e)}}{\partial y}\frac{\partial\phi_j^{(e)}}{\partial x}+A_{66}\frac{\partial\phi_i^{(e)}}{\partial y}\frac{\partial\phi_j^{(e)}}{\partial y}]dA$$

$$K_{ij}^{12(e)}=\int_{\Omega^{(e)}}[A_{12}\frac{\partial\phi_i^{(e)}}{\partial x}\frac{\partial\phi_j^{(e)}}{\partial y}+A_{16}\frac{\partial\phi_i^{(e)}}{\partial x}\frac{\partial\phi_j^{(e)}}{\partial x}+A_{26}\frac{\partial\phi_i^{(e)}}{\partial y}\frac{\partial\phi_j^{(e)}}{\partial y}+A_{66}\frac{\partial\phi_i^{(e)}}{\partial y}\frac{\partial\phi_j^{(e)}}{\partial x}]dA$$

$$K_{ij}^{21(e)}=\int_{\Omega^{(e)}}[A_{16}\frac{\partial\phi_i^{(e)}}{\partial x}\frac{\partial\phi_j^{(e)}}{\partial x}+A_{66}\frac{\partial\phi_i^{(e)}}{\partial x}\frac{\partial\phi_j^{(e)}}{\partial y}+A_{12}\frac{\partial\phi_i^{(e)}}{\partial y}\frac{\partial\phi_j^{(e)}}{\partial x}+A_{26}\frac{\partial\phi_i^{(e)}}{\partial y}\frac{\partial\phi_j^{(e)}}{\partial y}]dA$$

$$K_{ij}^{22(e)}=\int_{\Omega^{(e)}}[A_{26}\frac{\partial\phi_i^{(e)}}{\partial x}\frac{\partial\phi_j^{(e)}}{\partial y}+A_{66}\frac{\partial\phi_i^{(e)}}{\partial x}\frac{\partial\phi_j^{(e)}}{\partial x}+A_{22}\frac{\partial\phi_i^{(e)}}{\partial y}\frac{\partial\phi_j^{(e)}}{\partial y}+A_{26}\frac{\partial\phi_i^{(e)}}{\partial y}\frac{\partial\phi_j^{(e)}}{\partial x}]dA$$

$$F_i^{1(e)}=-\oint_{\Gamma_e} t_x\phi_i^{(e)}ds,\qquad F_i^{2(e)}=-\oint_{\Gamma_e} t_y\phi_i^{(e)}ds.$$

Equations (8) can be expressed with

$$\begin{bmatrix} K^{11(e)} & K^{12(e)} \\ K^{21(e)} & K^{22(e)} \end{bmatrix}\begin{Bmatrix} u^{(e)} \\ v^{(e)} \end{Bmatrix}=\begin{Bmatrix} F^{1(e)} \\ F^{2(e)} \end{Bmatrix}$$

and rearrange this system to get

$$[K^{(e)}]\{\Delta^{(e)}\}=\{F^{(e)}\}, \tag{10}$$

where

$$\{\Delta^{(e)}\}=[u_1^{(e)},v_1^{(e)},u_2^{(e)},v_2^{(e)},...u_n^{(e)},v_n^{(e)}]^T,$$

$$\{F^{(e)}\}=[F_1^{1(e)},F_1^{2(e)},F_2^{1(e)},F_2^{2(e)},...F_n^{1(e)},F_n^{2(e)}]^T.$$

The $[\ ]^T$ implies the transpose of the matrix [ ].

The interpolation equations below are applied for four-node rectangular element (see Figs 2);

$$\phi_1^e = (1-\frac{\bar{x}}{b_e})(1-\frac{\bar{y}}{a_e}), \qquad \phi_2^e = \frac{\bar{x}}{b_e}(1-\frac{\bar{y}}{a_e}), \qquad \phi_3^e = \frac{\bar{x}}{b_e}\frac{\bar{y}}{a_e}, \qquad \phi_4^e = (1-\frac{\bar{x}}{b_e})\frac{\bar{y}}{a_e},$$

and thus, after dropping the (e) superscript, we obtain

$$\left[K^{(e)}\right] = \begin{pmatrix} K_{11}^{11} & K_{11}^{12} & K_{12}^{11} & K_{12}^{12} & K_{13}^{11} & K_{13}^{12} & K_{14}^{11} & K_{14}^{12} \\ K_{11}^{21} & K_{11}^{22} & K_{12}^{21} & K_{12}^{22} & K_{13}^{21} & K_{13}^{22} & K_{14}^{21} & K_{14}^{22} \\ K_{21}^{11} & K_{21}^{12} & K_{22}^{11} & K_{22}^{12} & K_{23}^{11} & K_{23}^{12} & K_{24}^{11} & K_{24}^{12} \\ K_{21}^{21} & K_{21}^{22} & K_{22}^{21} & K_{22}^{22} & K_{23}^{21} & K_{23}^{22} & K_{24}^{21} & K_{24}^{22} \\ K_{31}^{11} & K_{31}^{12} & K_{32}^{11} & K_{32}^{12} & K_{33}^{11} & K_{33}^{12} & K_{34}^{11} & K_{34}^{12} \\ K_{31}^{21} & K_{31}^{22} & K_{32}^{21} & K_{32}^{22} & K_{33}^{21} & K_{33}^{22} & K_{34}^{21} & K_{34}^{22} \\ K_{41}^{11} & K_{41}^{12} & K_{42}^{11} & K_{42}^{12} & K_{43}^{11} & K_{43}^{12} & K_{44}^{11} & K_{44}^{12} \\ K_{41}^{21} & K_{41}^{22} & K_{42}^{21} & K_{42}^{22} & K_{43}^{21} & K_{43}^{22} & K_{44}^{21} & K_{44}^{22} \end{pmatrix}.$$

3. Results and Discussion

3.1. Stability of numerical approach

The stability of the finite element method adopted is displayed in Fig. 3 through the example below: A pair of partial differential operators in a rectangular domain $-1 \le x \le 1,\ -1 \le y \le 1,$

$$\frac{\partial}{\partial x}[(2\mu+\lambda)\frac{\partial u}{\partial x}+\lambda\frac{\partial v}{\partial y}]+\frac{\partial}{\partial y}[\mu(\frac{\partial u}{\partial y}+\frac{\partial v}{\partial x})] = \mu[4(y^2-1)+2(x^2-1)+4xy]+\lambda[2(y^2-1)+4xy]$$

$$\frac{\partial}{\partial x}[\mu(\frac{\partial v}{\partial x}+\frac{\partial u}{\partial y})]+\frac{\partial}{\partial y}[\lambda\frac{\partial u}{\partial x}+(2\mu+\lambda)\frac{\partial v}{\partial y}) = \mu[2(y^2-1)+4xy+4(x^2-1)]+\lambda[2(x^2-1)+4xy]$$

with boundary conditions

$\vec{u}(1,y)=0,\quad \vec{u}(-1,y)=0,\quad \vec{u}(x,1)=0,\quad \vec{u}(x,-1)=0,\quad \vec{u}(x,0)=0.$

For the value $\mu=\lambda=\frac{1}{2}$, the exact solution of the above example is $\begin{bmatrix} u \\ v \end{bmatrix} = \begin{bmatrix} (x^2-1)(y^2-1) \\ (x^2-1)(y^2-1) \end{bmatrix}.$

Figure 3(a) shows longitudinal displacement u for the representative discretized elemental numbers 2^3, 2^4, 2^5 and compared with exact solution. For the elemental number 2^3 some numerical error appears near the part of curve inflection,

while the approximate solutions are so close to the exact solution for the other elemental numbers. Similar characteristic behavior, as shown in Fig 3(b), occurs in the lateral displacement profile.

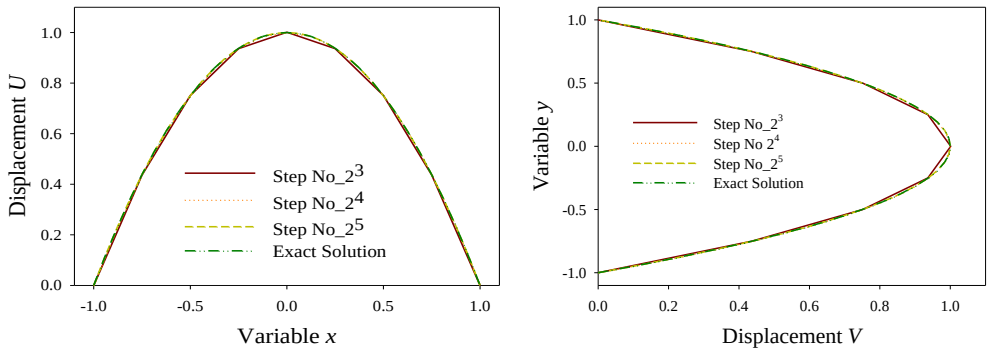

Figure 3. Displacement distribution profiles for stability: (a) longitudinal displacement, (b) lateral displacement

3.2. Numerical results

A panel of glass/epoxy laminated composite material is chosen for numerical study. Table 1 exhibits the mechanical properties of unidirectional glass /epoxy lamina. The laminated pile is composed of three ply with thickness 1mm and piled up in sequence [0/various angle/0]. The 1000Mpa pressure is applied to the guided panel as the maximum value, and all approximated solutions with discretized elemental number 2^4 are displayed to normalized position y/a at different sections $x/b=0.0$, $x/b=0.375$, $x/b=0.625$, and $x/b=0.875$.

Table 1. Mechanical properties of glass/epoxy

Property	E_1 (MPa)	E_2 (MPa)	G_{12} (MPa)	ν_{12}	ν_{21}
Value	38.6×10^3	8.27×10^3	4.14×10^3	0.26	0.06

Figures 4 and 5 exhibit the component profiles of displacement for the representative sequences [0/0/0] and [0/(π/4)/0], respectively. The normalized longitudinal displacement u_x/b, in Fig. 4(a), are presented to normalized position y/a corresponding to the aspect ratio of the panel $b/a=3.0$. The largest longitudinal displacement appears at the section $x/b=0.875$ and the magnitude decreases as the section value x/b approaches to zero. At the section $x/b=0.0$ no longitudinal displacement develops, which explains well the physical boundary condition. The longitudinal displacement components are extended to the positive direction in around $0\le y/a<0.5$, and move to the negative direction for the other values y/a. Fig. 4(b) displays the lateral displace-

ment components u_y/b to normalized position y/a. The lateral displacement develops to one direction only at the sections $x/b=0.375$ and $x/b=0.875$, while the curve of lateral displacement fluctuates to both negative and positive directions at the sections $x/b=0.625$. The largest magnitude of the lateral displacement occurs around $y/a=0.5$ at the sections $x/b=0.875$ and no displacement appears at the bottom and top of the panel.

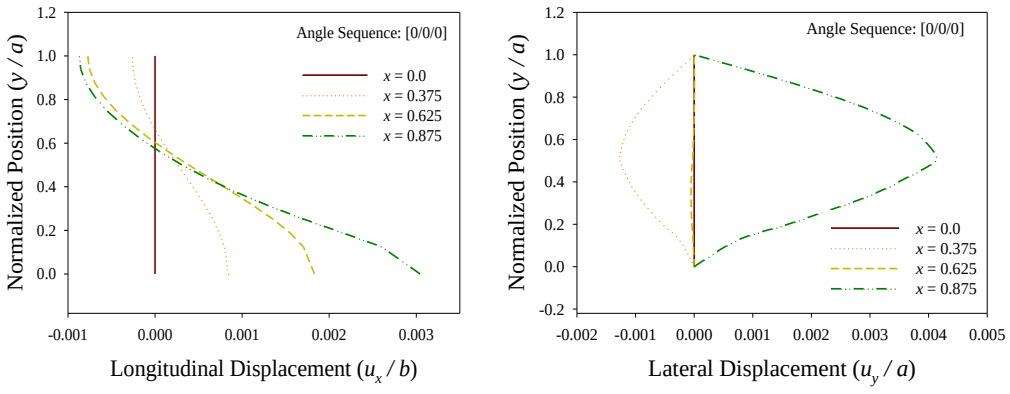

Figure 4. Displacement distribution profiles in the piling sequence [0/0/0]: (a) longitudinal displacement, (b) lateral displacement

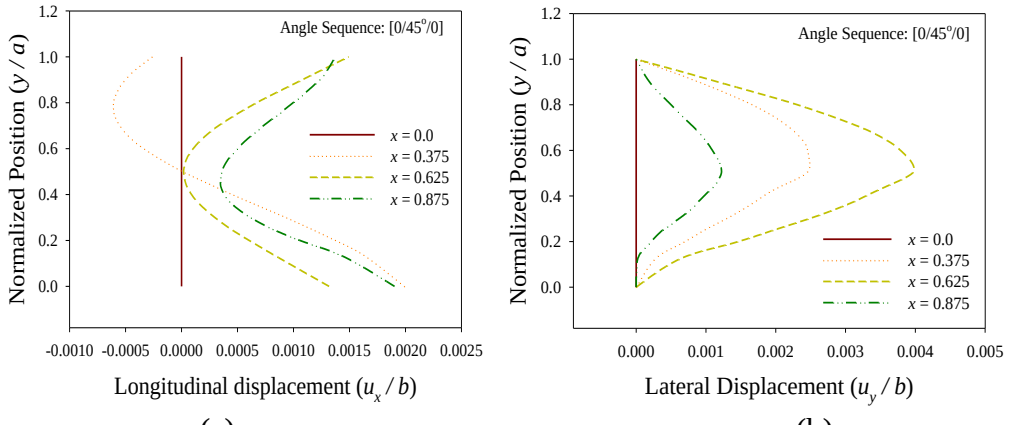

Figure 5. Displacement distribution profiles in the piling sequence $[0/(\pi/4)/0]$: (a) longitudinal displacement, (b) lateral displacement

Fig. 5(a) describes the longitudinal displacement components of the panel with laminated angle sequence $[0/(\pi/4)/0]$. The longitudinal displacement develops to the positive direction only at the sections $x/b=0.625$ and $x/b=0.875$, but the section $x/b=0.375$ extends to both positive and negative directions. The largest longitudinal displacement appears at the bottom of the section $x/b=0.375$, and the smallest longitudinal displacement occurs at the center of the normalized position

y/a. At the section $x/b=0.0$, no longitudinal displacement develops, which satisfies the physical boundary conditions. Fig. 5(b) presents the lateral displacement for the laminated angle sequence $[0/(\pi/4)/0]$. The components of the lateral displacement are discovered in the positive area for the sections $x/b=0.375$, $x/b=0.625$, and $x/b=0.875$, and the largest displacement is found at the center of the normalized position y/a of the section $x/b=0.625$. At the section $x/b=0.0$, the lateral displacement is trivial.

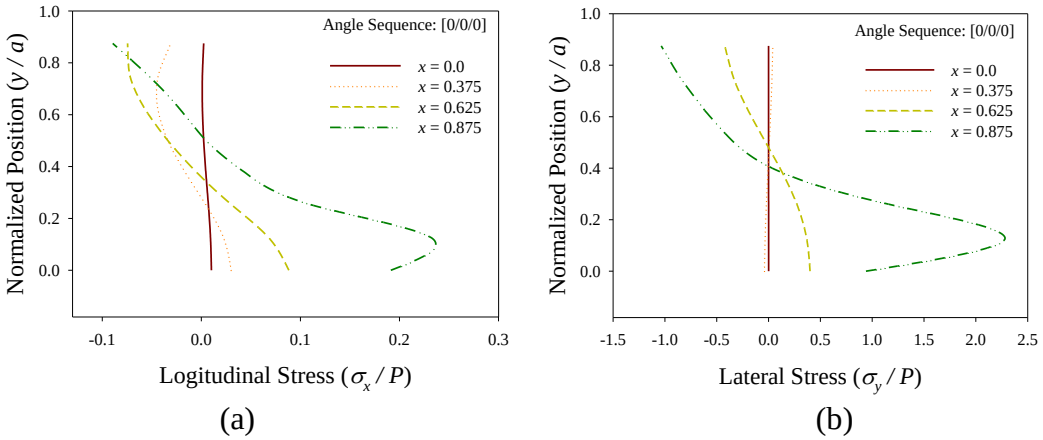

Figure 6. Stress distribution profiles in the piling sequence [0/0/0]: (a) longitudinal stress, (b) lateral stress

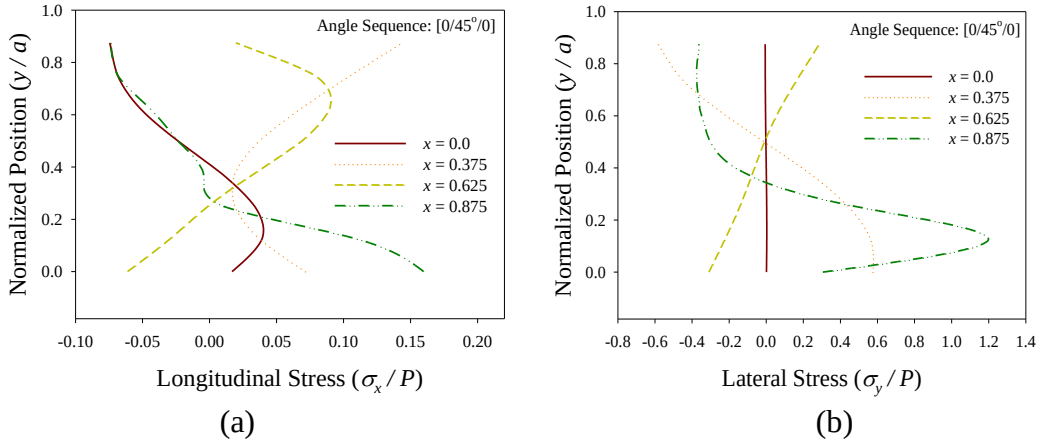

Figure 7. Stress distribution profiles in the piling sequence $[0/(\pi/4)/0]$: (a) longitudinal stress, (b) lateral stress

The stress profiles are displayed figures 6-7, and the components of stresses are expressed with normalized position y/a corresponding to the aspect ratio of the roller guided panel $b/a=3.0$. The longitudinal stress σ_x/P for the sequence [0/0/0] is shown in Fig. 6(a). For all sections, the compressive longitudinal stress is appeared near the top part of the panel, whereas the bottom

part of the panel is under the action of tension. The largest magnitude of the longitudinal stress happens around $y/a = 0.1$ of the section $x/b = 0.875$, and the magnitude decreases as the value x/b approaches to zero. Figure 6(b) indicates the distribution profiles of lateral stress for the sequence [0/0/0]. At the both sections $x/b = 0.625$, and $x/b = 0.875$, the behavior is similar to the characteristics of the longitudinal stress except stress magnitude, that is, the top and bottom areas of the roller guided panel is under the constraint of compression and tension, respectively. However, the movement of lateral stress at the section $x/b = 0.375$ is opposite to the behavior of longitudinal stress. The magnitude of the both longitudinal and lateral stress may be ignorable at the section $x/b = 0.0$. Through the results of stresses, it is recognized that the roller guided panel is under a loading of distortion. The distribution profiles of stresses for the sequence $[0/(\pi/4)/0]$ are presented in Fig. 6. As shown Fig. 7(a) the longitudinal stress is not ignorable at the section $x/b = 0.0$, and lower part of the panel is under a loading of tension and upper area is subjected to compression. On the other hand, a compressive longitudinal stress develops at the lower part and upper part is influenced with a tensile longitudinal stress at the section $x/b = 0.625$. The section $x/b = 0.375$ undergoes tensile longitudinal stress only and the largest tensile and compressive stresses, respectively, occur at the bottom and top of the roller guided panel. Fig. 7(b) displays the lateral stress distribution profiles. Unlike longitudinal stress, negligible lateral stress develops at the section $x/b = 0.0$. Moreover, the largest tensile lateral stress appears around $y/a = 0.1$ of the section $x/b = 0.875$, and the top point of the section $x/b = 0.375$ generates the highest compressive lateral stress. The lower part of $x/b = 0.625$ is under the action of compression, while the top area is subject to tensile lateral stress. The elastic characteristics of the roller guided panel, according to the results, are so sensitive to the laminated sequence.

Figure 8 describes the longitudinal stress distribution profiles for the various laminate sequences [0/0/0], $[0/(\pi/8)/0]$, $[0/(\pi/6)/0]$, $[0/(\pi/4)/0]$, and $[0/(\pi/2)/0]$. The representative sections $x/b = 0.375$, $x/b = 0.625$, and $x/b = 0.875$ are chosen to compare the elastic characteristics of each section. At the section $x/b = 0.375$, the lamina with sequences $[0/(\pi/6)/0]$, $[0/(\pi/4)/0]$, and $[0/(\pi/2)/0]$ are under of tensile longitudinal loading only (see Fig. 8(a)). However, the lamina with sequences [0/0/0] and $[0/(\pi/8)/0]$ are affected with both compressive and tensile longitudinal loading. The lamina with sequence [0/0/0] is subject to tension for the interval $0.0 \le y/a < 0.3$ and compressive longitudinal pressure develops for the other values of y/a. The behavior of the lamina with sequence $[0/(\pi/8)/0]$ is opposite to the lamina of [0/0/0]. The largest tensile longitudinal stress is obtained at the top point of the lamina of $[0/(\pi/4)/0]$, whereas the lamina with sequence $[0/(\pi/8)/0]$ creates the largest compressive longitudinal stress at the bottom point.

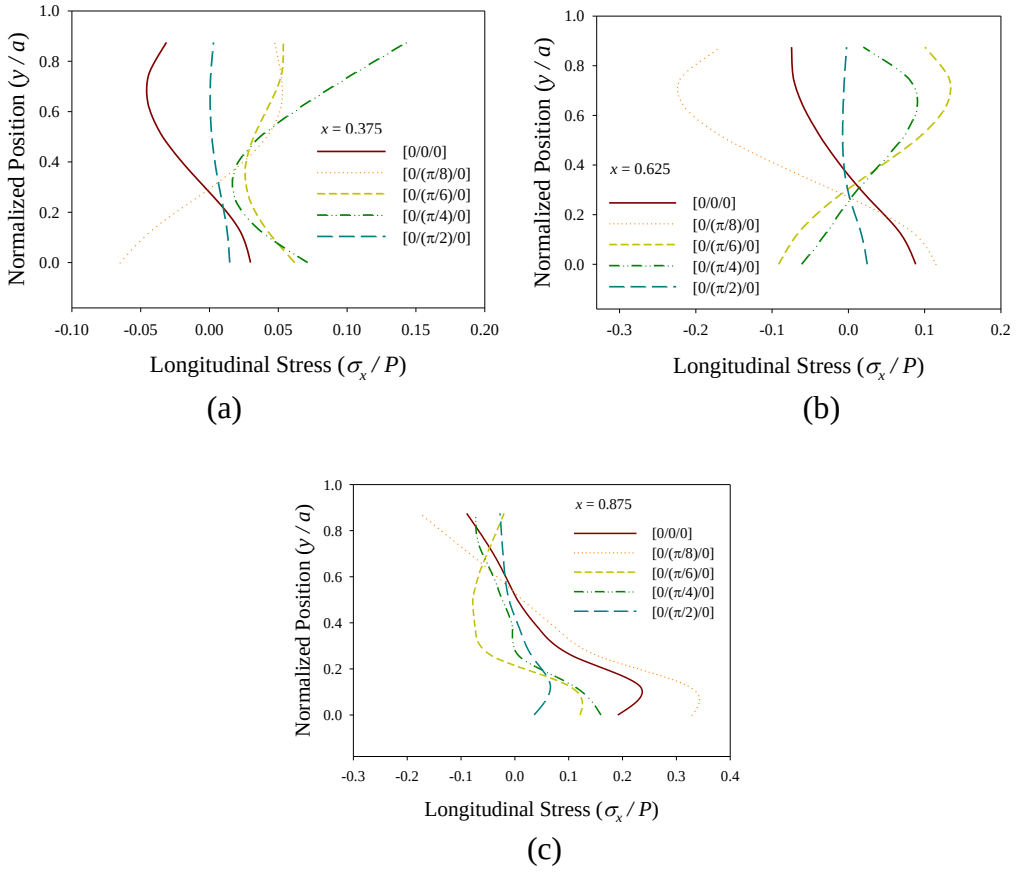

Figure 8. Longitudinal stress distribution profiles for various piling sequences at: (a) $x/b = 0.375$, (b) $x/b = 0.625$, (c) $x/b = 0.875$

As shown in Fig. 8(b), all roller guided panels are under the pressure of both tension and compression at the section $x/b = 0.625$. The panels of the lamina with sequences [0/0/0], $[0/(\pi/8)/0]$, and $[0/(\pi/2)/0]$ develop tensile stress at the lower part and the tensile stress converts into compression at the upper part. However, opposite behavior appears for the panels of the lamina with sequences $[0/(\pi/6)/0]$ and $[0/(\pi/4)/0]$. The largest tensile stress occurs around $y/a = 0.7$ of the panel of $[0/(\pi/6)/0]$, while the panel of $[0/(\pi/2)/0]$ is influenced with the largest compressive stress around $y/a = 0.7$. The distribution profiles of longitudinal stress at the section $x/b = 0.875$ are expressed in Fig. 8(c). All laminas are experienced of tension at the lower area and compression at the upper area. The panel of lamina with sequence $[0/(\pi/8)/0]$ undergoes the largest tensile stress happens around $y/a = 0.1$ and the largest compressive stress at the top point. The stress variation range of the panel with sequence $[0/(\pi/2)/0]$ is smallest among them.

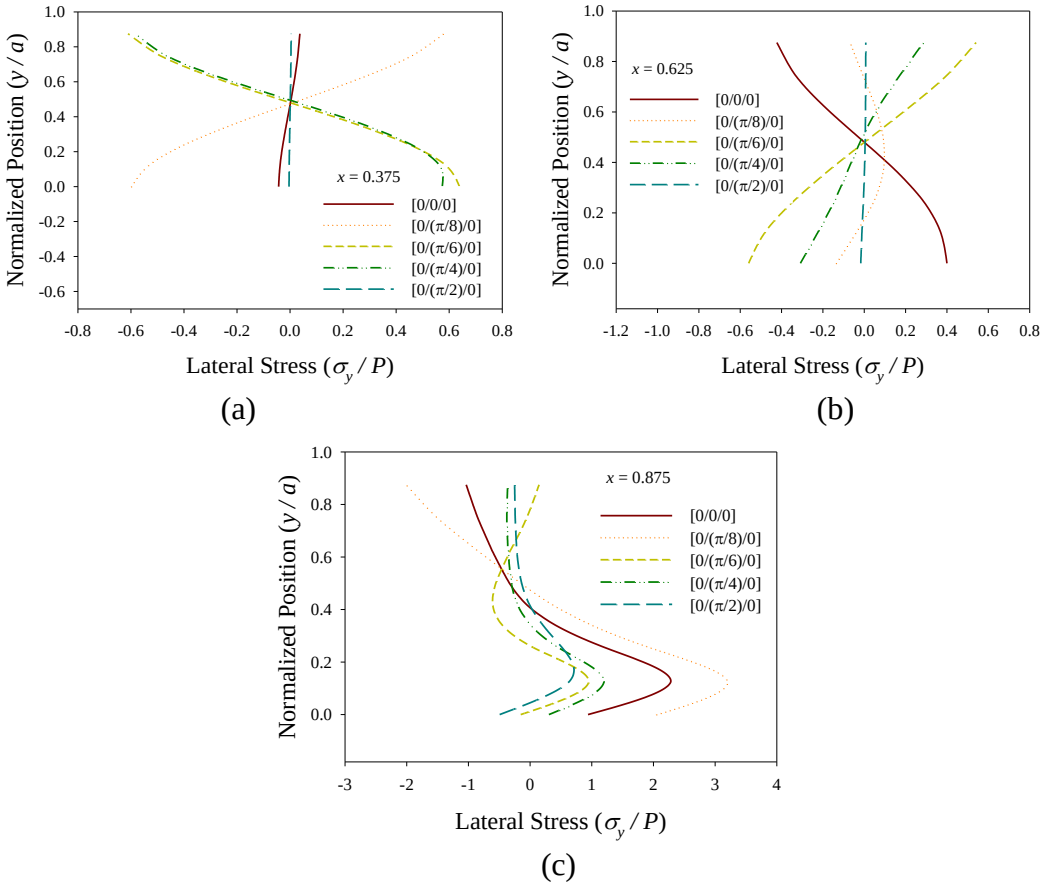

Figure 9. Lateral stress distribution profiles for various piling sequences at: (a) $x/b = 0.375$, (b) $x/b = 0.625$, (c) $x/b = 0.875$

The lateral stress distribution profiles are displayed in Fig. 9. The lamina with sequences $[0/(\pi/6)/0]$, $[0/(\pi/4)/0]$, and $[0/(\pi/2)/0]$ are taken into account and the representative sections chosen are $x/b = 0.375$, $x/b = 0.625$, and $x/b = 0.875$. At the section $x/b = 0.375$, the range of lateral stress variation of the lamina with sequence $[0/(\pi/2)/0]$ is trivial in comparing with the others (see Fig. 9(a)). The laminas with sequence [0/0/0] and $[0/(\pi/8)/0]$ are subject to comprehensive lateral stress at the lower area of the panel and upper area is under the loading of tension. Meanwhile, tensile lateral stress develops at the lower part of the panel of sequence $[0/(\pi/6)/0]$ and $[0/(\pi/4)/0]$, and compressive lateral stress at the upper part. The bottom point of the panel of sequence $[0/(\pi/6)/0]$ experiences of the highest tensile stress and the lowest compressive stress is obtained at the bottom point of the panel of sequence $[0/(\pi/8)/0]$. Fig. 9(b) presents the lateral stress distribution profiles at the section $x/b = 0.625$. Similarly, the lateral stress of the lamina with sequence $[0/(\pi/2)/0]$ varies within a small range. The upper and lower areas of the panel of sequence $[0/(\pi/8)/0]$ are under of compressive pressure and tensile lateral stress appears at the middle part,

which yields a parabolic shape in the lateral stress movement. The panels with sequence $[0/(\pi/6)/0]$ and $[0/(\pi/4)/0]$ are under the constraint of compression at the lower part, whereas the panel with sequence [0/0/0] suffers from of tensile lateral stress. The behavior of lateral stress at the section $x/b = 0.875$ is volatile in comparing with the other section (see Fig. 9(c)). Specially, the lateral stress of the panels with sequence $[0/(\pi/6)/0]$ fluctuates rhythmically from compression and tension and forms a sinus shape. The lateral stress panels with sequence $[0/(\pi/8)/0]$ varies within the largest range, and the largest tensile stress is found at the around $y/a = 0.1$ and the top point shows the largest compressive stress.

4. Conclusion

The elastic behaviors of roller-guided panel symmetrically cross-ply laminated composite field were investigated by Afsar et. al. [13] using particular solution. But, due to the complexity of the governing equations, no author presents the elastic characteristics of non-symmetric cross-ply laminated composite field guided by roller panel. The elastic characteristics have been analyzed to non-symmetric cross-ply laminated composite field guided by roller panel for various laminas, consisting of different angle sequence. It is recognized that the movement of the roller guided panel are so sensitive to the laminated sequence and the laminated angle is a crucial factor to control the elastic movement. Moreover, the various behaviors appear depending on the section of a laminated elastic field and the manner of loading to elastic field play important role to determine of the elastic characteristics. The mathematical approach, through the results exhibited, is reasonable and acceptable, and the results may be helpful to design ideally laminated elastic field.

Acknowledgements. This research was supported by Basic Science Research Program through the National Research Foundation of Korea (NRF) funded by the Ministry of Education (2013R1A1A2059235). [2]This work was supported by the National Research Foundation of Korea (NRF) grant funded by the Korea government (MSIP) (2011-0030058).

References

[1] S. Sridharan, A. Kasagi, On the buckling and collapse of moderately thick composite cylinders under hydrostatic pressure, *Composites Part B: Engineering*, **28** (1997), 583–596. http://dx.doi.org/10.1016/s1359-8368(96)00072-8

[2] P. Davies, P. Chauchot, Composites for marine applications – part 2: Underwater structures, Chapter in *Mechanics of Composite Materials and Structures*, Dordrecht: Kluwer Academic Publishers, Vol. 361, 1999, 249-260. http://dx.doi.org/10.1007/978-94-011-4489-6_13

[3] J.S. Anastasiadis, G.J. Simitses, Buckling of pressure-loaded, long, shear deformable cylindrical laminated shells, *Comput. Structures*, **23** (1993), 221–231. http://dx.doi.org/10.1016/0263-8223(93)90224-e

[4] D.H. Hodges, Non-linear inplane deformation and buckling of rings and high arches, *Int. Journal of Non-Linear Mechanics*, **34** (1999), 723–737. http://dx.doi.org/10.1016/s0020-7462(98)00050-x

[5] Karam Y. Maalawi, Use of material grading for enhanced buckling design of thin-walled composite rings/long cylinders under external pressure, *Composite Structures,* **93** (2011), 351–359. http://dx.doi.org/10.1016/j.compstruct.2010.09.007

[6] W.T. Wang, T.Y. Kam, Material characterization of laminated composite plates via static testing, *Composite Structures*, **50** (2000), 347–352. http://dx.doi.org/10.1016/s0263-8223(00)00112-4

[7] S. Salim, D. Yadav, N.G.R. Iyengar, Analysis of composite plates with random material characteristics, *Mech. Res. Commun.*, **20** (1993), 405–414. http://dx.doi.org/10.1016/0093-6413(93)90031-i

[8] D.J. Gorman, Free vibration analysis of rectangular plates with nonuniform lateral elastic edge support, *Appl. Mech. Rev.*, **60** (1993), 998–1003. http://dx.doi.org/10.1115/1.2901015

[9] B.N. Raj, N.G.R. Iyengar, D. Yadav, Response of composite plates with random material properties using FEM Monte Carlo Simulation, *Adv. Compos. Materials*, **7** (1998), 219–237. http://dx.doi.org/10.1163/156855198x00165

[10] S. Nakagiri, H. Takabatake, S. Tani, Uncertain eigenvalue analysis of composite laminated plates by the Stochastic Finite Element Method, *Journal of Engineering for Industry*, **109** (1987), 9–12. http://dx.doi.org/10.1115/1.3187096

[11] G. Singh, G. Venkateswara Rao, N.G.R. Iyengar, Non-linear forced vibrations of antisymmetric rectangular cross-ply plates, *Composite Structures*, **20** (1992), 185–194. http://dx.doi.org/10.1016/0263-8223(92)90025-8

[12] Amit Kumar Onkar, D. Yadav, Forced nonlinear vibration of laminated composite plates with random material properties, *Composite Structures*, **70** (2005), 334-342. http://dx.doi.org/10.1016/j.compstruct.2004.08.037

[13] A.M. Afsar, N.M.L. Huq, J.L. Song, Analytical solution to a mixed boundary value elastic problem of a roller-guided panel of laminated composite, *Arch. Appl. Mech.*, **80** (2010), 401-402. http://dx.doi.org/10.1007/s00419-009-0324-z

Received: April 21, 2016; Published: June 12, 2016